

CONSTRUCTING LAGRANGIANS FROM TRIPLE GRID DIAGRAMS

SARAH BLACKWELL, DAVID GAY, AND PETER LAMBERT-COLE

ABSTRACT. Links in S^3 can be encoded by grid diagrams; a grid diagram is a collection of points on a toroidal grid such that each row and column of the grid contains exactly two points. Grid diagrams can be reinterpreted as front projections of Legendrian links in the standard contact 3–sphere. In this paper, we define and investigate triple grid diagrams, a generalization to toroidal diagrams consisting of horizontal, vertical, and diagonal grid lines. In certain cases, a triple grid diagram determines a closed Lagrangian surface in $\mathbb{C}\mathbb{P}^2$. Specifically, each triple grid diagram determines three grid diagrams (row-column, column-diagonal and diagonal-row) and thus three Legendrian links, which we think of collectively as a Legendrian link in a disjoint union of three standard contact 3–spheres. We show that a triple grid diagram naturally determines a Lagrangian cap in the complement of three Darboux balls in $\mathbb{C}\mathbb{P}^2$, whose negative boundary is precisely this Legendrian link. When these Legendrians are maximal Legendrian unlinks, the Lagrangian cap can be filled by Lagrangian slice disks to obtain a closed Lagrangian surface in $\mathbb{C}\mathbb{P}^2$. We construct families of examples of triple grid diagrams and discuss potential applications to obstructing Lagrangian fillings.

1. INTRODUCTION AND MAIN STATEMENTS

This paper concerns combinatorial descriptions of Lagrangian surfaces in $\mathbb{C}\mathbb{P}^2$, analogous to grid diagrams as combinatorial descriptions of Legendrian links in S^3 . The connection between the two settings is tied to the fact that S^3 has a genus one Heegaard splitting in which the α curve is “vertical” and the β curve is “horizontal,” while $\mathbb{C}\mathbb{P}^2$ has a genus one trisection [GK16] in which the α curve is “vertical,” the β curve is “horizontal,” and the γ curve is “diagonal” with slope -1 (see Figure 1). Taking multiple parallel copies of these curves gives a grid on T^2 on which we can place marked points which encode these Legendrians or Lagrangians.

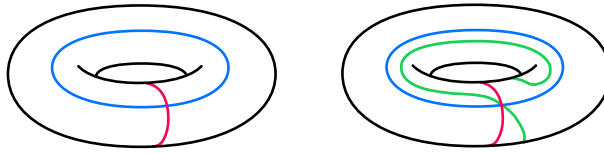


FIGURE 1. A genus one Heegaard splitting of S^3 (left) and a genus one trisection of $\mathbb{C}\mathbb{P}^2$ (right).

We define two slightly (but crucially) different versions of triple grid diagrams arising from this setup, which are each useful in various contexts. Grid diagrams for links in S^3 are generally considered to be discrete, combinatorial objects. It is therefore useful to define a combinatorial object mimicking the application of grid diagrams to the study of Legendrian links. However Lagrangian surfaces are geometric objects that may live in moduli spaces and important geometric properties – the symplectic action, monotonicity, and holomorphic disk counts – are not invariant under small perturbations.

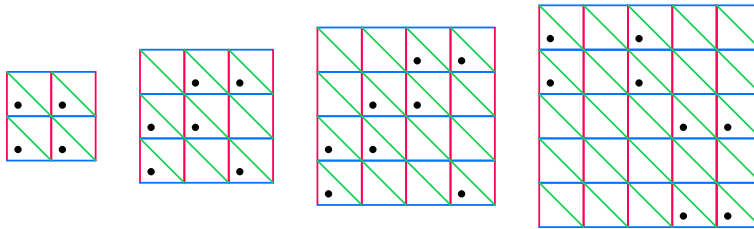


FIGURE 2. Some examples of combinatorial triple grid diagrams.

The following definition first appears in the first author's PhD thesis [Bla22].

Definition 1.1. A *combinatorial triple grid diagram* of grid number n and size b consists of:

- (1) a grid on the torus $T^2 = \mathbb{R}^2/\mathbb{Z}^2$ consisting of three sets of lines:
 - (a) n vertical lines $\{x = \frac{k}{n} : 1 \leq k \leq n\}$, colored red by convention,
 - (b) n horizontal lines $\{y = \frac{k}{n} : 1 \leq k \leq n\}$, colored blue by convention, and
 - (c) n diagonal lines (of slope -1) $\{x + y = \frac{k}{n} : 1 \leq k \leq n\}$, colored green by convention.
- (2) $2b$ points in the complement of the $3n$ grid lines, such that in the region between any pair of adjacent lines of the same slope, there are exactly zero or two points.

See Figure 2, and further, Section 4.2, for several examples. Each red-blue square is divided by a green diagonal into two triangles. By convention we only place dots in the lower left triangles. We often draw these diagrams as squares where opposite edges are identified; hence the diagonals wrap around, so that there are exactly n diagonals.

Definition 1.2. A *geometric triple grid diagram* is a collection Θ of $2b$ points on the torus $T^2 = \mathbb{R}^2/\mathbb{Z}^2$ such that for any vertical line $\{x = c\}$, any horizontal line $\{y = c\}$, or any diagonal line $\{x + y = c\}$, exactly zero or two points of Θ lie on the line.

A combinatorial triple grid diagram immediately determines a geometric triple grid diagram, by forgetting the grid lines. Conversely, after possibly a small perturbation, it is possible to draw grid lines disjoint from a geometric triple grid diagram if the grid size n is sufficiently large. For the purposes of the results that follow, either form of triple grid diagram suffices to make the statements correct, but the actual constructions start from the explicit data of the $2b$ points of a geometric triple grid diagram.

Following the work of Meier and Zupan [MZ17; MZ18] on bridge trisections, and the further developments in [HKM20; GM22], note that a combinatorial triple grid diagram can be thought of as a special kind of multi-pointed Heegaard triple describing a bridge trisected surface, and when the points of a geometric triple grid diagram are connected horizontally, vertically and diagonally, the result can be thought of as a shadow diagram for such a surface (provided, in both cases, that all three links described by the triple grid diagram are unlinks). Furthermore, symplectic surfaces in $\mathbb{C}\mathbb{P}^2$ were characterized in terms of *transverse bridge position* by the third author in [Lam23].

We first provide executive summaries of the main results and then give more explicit details after. As we will see below, a triple grid diagram determines three Legendrian links in three copies of the standard contact S^3 , which we identify as the boundaries of three disjoint standard balls in $\mathbb{C}\mathbb{P}^2$.

Theorem 1.3 (Executive summary). *A triple grid diagram D determines a properly embedded Lagrangian surface $L(D)$ in the complement of these three balls which is a Lagrangian cap for the disjoint union of the three associated Legendrians, in the sense of intersecting each S^3 in the given Legendrian and being tangent to inward pointing Liouville vector fields near each S^3 .*

Corollary 1.4 (Executive summary). *When the three Legendrian links associated to diagram D are all Legendrian unlinks of Legendrian unknots of Thurston-Bennequin number $tb = -1$, then $L(D)$ can be filled with disjoint Lagrangian disks to give a closed, embedded Lagrangian surface $\bar{L}(D)$ in $\mathbb{C}\mathbb{P}^2$ determined by D .*

Note that an outline of a proof of this corollary appears in [Bla22], and the proof in this paper essentially follows the same ideas but has a slightly different organization.

We now give a more explicit setup that allows us to state these results precisely. By convention, the vertical lines in the grid are colored red and called α curves, the horizontal lines are colored blue and called β curves, and when we draw the slope -1 grid lines these are colored green and called γ curves. Note that there is an order 3 element of $SL_2\mathbb{Z}$, i.e. an order 3 orientation preserving automorphism of T^2 , which cyclically permutes (α, β, γ) . Thus, by applying this automorphism, we can choose to view any pair of colors as horizontal and vertical, as long as the cyclic order is preserved. In other words, we can make β vertical, γ horizontal and α diagonal, or we can make γ vertical, α horizontal and β diagonal.

For each pair of colors we get a link diagram by first cyclically permuting until that pair of colors are horizontal and vertical, then connecting dots horizontally and vertically by straight line segments, and then adopting the convention that horizontal segments pass over vertical segments when they cross. Now by rotating this diagram 45° clockwise and either smoothing corners or replacing corners with cusps so as to avoid vertical tangencies, we obtain a front diagram for a Legendrian link in S^3 . We will call this the *standard Legendrianization of a grid diagram*. Thus each triple grid diagram D gives three Legendrian links $\Lambda_{\alpha\beta}(D)$, $\Lambda_{\beta\gamma}(D)$ and $\Lambda_{\gamma\alpha}(D)$, which we think of as living in three different copies of the standard contact (S^3, ξ) , labelled $(S^3_{\alpha\beta}, \xi_{\alpha\beta})$, $(S^3_{\beta\gamma}, \xi_{\beta\gamma})$ and $(S^3_{\gamma\alpha}, \xi_{\gamma\alpha})$, respectively. This whole process is illustrated in Figure 3.

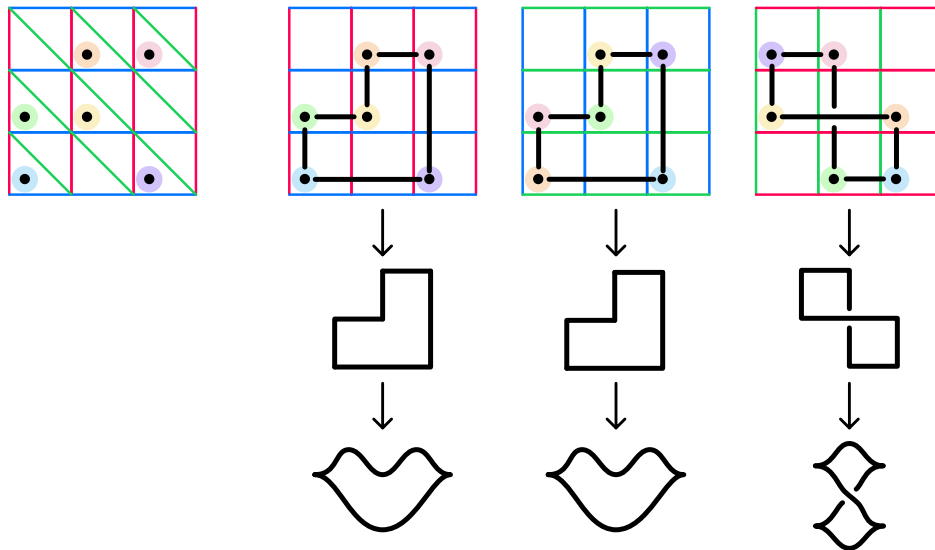


FIGURE 3. A (combinatorial) triple grid diagram. The right-hand side shows separately the three grids making up the triple grid diagram on the left-hand side, along with the knot represented by each grid. Colors are used to indicate where each vertex in the triple grid diagram shows up in the three individual grids. Below the grids the process for obtaining Legendrians is shown.

Also naturally associated to a triple grid diagram D is an abstract trivalent graph $\Gamma(D)$ with edges colored red, blue and green (or labelled α , β or γ) where the vertices are the dots in the diagram and two dots are connected by an appropriately colored/labelled edge when they lie in the same row, column or diagonal. See for instance Figure 4. The edges at each vertex are cyclically ordered by the (α, β, γ) order, and we use this to construct an abstract “ribbon” surface $R(D)$ which is a thickening of $\Gamma(D)$. Note that this is not the standard “fat graph” construction coming from a cyclic ordering of edges at each vertex, since this standard construction produces an orientable surface, whereas $R(D)$ may or may not be orientable.

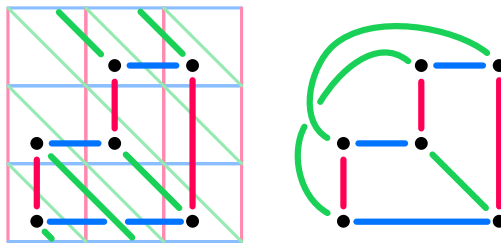


FIGURE 4. The trivalent graph $\Gamma(D)$ associated to the triple grid diagram D shown in Figure 3. The left-hand side depicts the graph still on the grid, with the green edges wrapping around the torus, while the right-hand side depicts the graph abstractly.

Begin with an oriented copy of D_v^2 for each vertex v of $\Gamma(D)$ and attach an *orientation-reversing*, that is, *half-twisted*, band from D_v^2 to D_w^2 whenever there is an edge from v to w , with the band colored/labelled the same as its corresponding edge. Attach these bands in order red, blue, green going clockwise around the boundary of each D_v^2 . We discuss orientability of $R(D)$ in more detail in Section 4. Note that the boundary of $R(D)$ is naturally the disjoint union of three 1-manifolds $\partial_{\alpha\beta}R(D)$, $\partial_{\beta\gamma}R(D)$ and $\partial_{\gamma\alpha}R(D)$, based on the pairs of colors making up each component of $\partial R(D)$.

In $\mathbb{C}\mathbb{P}^2$ with projective coordinates $\{[z_1 : z_2 : z_3]\}$, consider the three disjoint closed balls:

$$\begin{aligned} B_1 &= \{[z_1 : z_2 : 1] \mid |z_1|^2 + |z_2|^2 \leq \frac{1}{5}\}, \\ B_2 &= \{[z_1 : 1 : z_3] \mid |z_1|^2 + |z_3|^2 \leq \frac{1}{5}\}, \\ B_3 &= \{[1 : z_2 : z_3] \mid |z_2|^2 + |z_3|^2 \leq \frac{1}{5}\}. \end{aligned}$$

(The exact sizes are not important except that they should be small enough to accommodate an explicit construction given later, and $\frac{1}{5}$ is small enough.) Endow $\mathbb{C}\mathbb{P}^2$ with the standard symplectic form ω (which we express later in toric coordinates), and then let $X = \mathbb{C}\mathbb{P}^2 \setminus \text{int}(B_1 \cup B_2 \cup B_3)$, so that (X, ω) is a symplectic 4-manifold with three concave (hence contact) S^3 boundary components $(\partial_1 X, \xi_1)$, $(\partial_2 X, \xi_2)$, $(\partial_3 X, \xi_3)$. Each of these contact structures ξ_i is induced by a standard radial Liouville vector field V_i on B_i , pointing in along $\partial_i X$, and thus each $(-\partial_i X, \xi_i)$ is contactomorphic to the standard contact (S^3, ξ) .

Now we can restate our main theorem.

Theorem 1.3 (Restated more precisely). *Given any triple grid diagram D there exists a properly embedded Lagrangian surface $L(D) \subset (X, \omega)$ satisfying the following properties.*

- (1) *In a neighborhood of each $\partial_i X$, $L(D)$ is tangent to V_i , so that $L(D) \cap \partial_i X$ is a Legendrian link Λ_i in $(-\partial_i X, \xi_i)$ in X .*

(2) There are contactorphisms taking Legendrian links to Legendrian links as follows:

$$\begin{aligned} (-\partial_1 X, \xi_1, \Lambda_1) &\rightarrow (S_{\alpha\beta}^3, \xi_{\alpha\beta}, \Lambda_{\alpha\beta}), \\ (-\partial_2 X, \xi_2, \Lambda_2) &\rightarrow (S_{\beta\gamma}^3, \xi_{\beta\gamma}, \Lambda_{\beta\gamma}), \\ (-\partial_3 X, \xi_3, \Lambda_3) &\rightarrow (S_{\gamma\alpha}^3, \xi_{\gamma\alpha}, \Lambda_{\gamma\alpha}). \end{aligned}$$

(3) $L(D)$ is diffeomorphic to the abstract surface $R(D)$, via a diffeomorphism taking Λ_1 to $\partial_{\alpha\beta}R(D)$, Λ_2 to $\partial_{\beta\gamma}R(D)$ and Λ_3 to $\partial_{\gamma\alpha}R(D)$.

In short, $L(D)$ is a Lagrangian cap in X for $\Lambda_{\alpha\beta} \sqcup \Lambda_{\beta\gamma} \sqcup \Lambda_{\gamma\alpha}$. We will call such a cap – that which caps off a disjoint union of three Legendrians in three S^3 's – a *triple cap*.

Finally we can restate, and prove, our main corollary.

Corollary 1.4 (Restated more precisely). *A triple grid diagram D for which each of the three Legendrian links $\Lambda_{\alpha\beta}(D)$, $\Lambda_{\beta\gamma}(D)$ and $\Lambda_{\gamma\alpha}(D)$ is a Legendrian unlink of Legendrian unknots with Thurston-Bennequin number $tb = -1$ determines a closed embedded Lagrangian surface $\bar{L}(D)$ in $\mathbb{C}\mathbb{P}^2$ diffeomorphic to the result of attaching a disk to each boundary component of $R(D)$.*

Proof. The Legendrian unlink of Legendrian unknots with $tb = -1$ has a filling in B^4 by disjoint Lagrangian disks (Proposition 2.9) and these fillings can be glued (via Proposition 2.8) to the triple cap produced in Theorem 1.3. \square

Remark 1.5. More generally, as pointed out by our referee, whenever all three Legendrian links $\Lambda_{\alpha\beta}(D)$, $\Lambda_{\beta\gamma}(D)$ and $\Lambda_{\gamma\alpha}(D)$ are Lagrangian fillable we can glue the fillings to our triple cap to produce a closed Lagrangian surface.

We can also obtain immersed surfaces from triple grid diagrams under more general conditions.

Corollary 1.6. *Let D be a triple grid diagram such that each component of each of the three Legendrian links $\Lambda_{\alpha\beta}(D)$, $\Lambda_{\beta\gamma}(D)$ and $\Lambda_{\gamma\alpha}(D)$ has rotation number 0. Then D determines an immersed Lagrangian surface $\bar{L}(D)$ in $\mathbb{C}\mathbb{P}^2$ obtained by gluing immersed Lagrangian disks to the boundary components of $R(D)$.*

Proof. The proof is identical to the proof of Corollary 1.4, except using the immersed Lagrangian fillings from Proposition 2.12. \square

Further directions. In this paper, we focused on the triple grid diagrams compatible with the standard toric structure on $\mathbb{C}\mathbb{P}^2$. The three grid slopes $(0, 1, \infty)$ are determined by the slopes of the boundaries of the compressing disks on T^2 . More generally, there exists almost-toric fibrations on $\mathbb{C}\mathbb{P}^2$ (indexed by Markov triples) that yield decompositions into three rational homology 4-balls. These almost-toric fibrations can be encoded by a triple of compressing slopes as well. Specifically, if (a, b, c) is a Markov triple and we view α, β, γ as vectors in \mathbb{Z}^2 , then the three compressing slopes are determined, modulo the action of $SL(2, \mathbb{Z})$, by the equation

$$a^2\alpha + b^2\beta + c^2\gamma = 0$$

Therefore, just as grid diagrams for (Legendrian) knots in S^3 generalize to knots in lens spaces, there is an immediate generalization of triple grid diagrams to these decompositions arising from almost-toric fibrations. Etnyre, Min, Piccirillo and Roy recently reinterpreted these almost-toric fibrations as small symplectic caps of triples of universally tight contact structures on lens spaces [Etn+23]. A triple grid diagram should naturally determine a Lagrangian cap in these small symplectic caps.

In a future paper we will discuss the uniqueness of our constructions up to Hamiltonian isotopy; this is a subtle issue because, as mentioned above, Lagrangians are geometric objects which are sensitive to small perturbations. We will also discuss the extent to which Lagrangians “occurring in nature” can be shown to be Hamiltonian isotopic to Lagrangians constructed from triple grid diagrams, as well as the natural question of enumerating moves on triple grid diagrams that allow us to move between different triple grid diagrams representing appropriately “equivalent” Lagrangians.

Outline. In [Section 2](#) we give some background on Lagrangian fillings and caps of Legendrians, and in particular prove the propositions needed for the proofs of [Corollary 1.4](#) and [Corollary 1.6](#). In [Section 3](#) we show how to construct triple caps from triple grid diagrams, proving [Theorem 1.3](#). Finally, in [Section 4](#) we discuss various examples and applications.

Acknowledgments. All three authors would like to thank the Max Planck Institute for Mathematics for generous hospitality in 2019-20 when much of this work was initiated, the first author for the support of a postdoctoral position in 2022-23, and the second author for support during a visit in 2023. We also would like to sincerely thank the anonymous referees for their careful reading of our paper and their insightful comments. All three authors were supported by NSF Focused Research Group grant DMS-1664567 “FRG: Collaborative Research: Trisections – New Directions in Low-Dimensional Topology”. The second author was supported by NSF grant DMS-2005554 “Smooth 4-Manifolds: 2-, 3-, 5- and 6-Dimensional Perspectives”.

2. LAGRANGIAN COBORDISMS, FILLINGS, AND CAPS

In this section, we review the background material on Lagrangian fillings and caps and state the gluing result ([Proposition 2.8](#)). We also describe Lagrangian disk fillings in the cases of maximal Legendrian unlinks and immersed Lagrangian links where each component has rotation number 0. Combining these Lagrangian fillings with the Lagrangian caps constructed in the previous section and the gluing result completes the proof of [Corollary 1.4](#).

2.1. Basic definitions. To motivate the construction, we recall some terminology and facts about Lagrangian fillings of Legendrian links.

Definition 2.1. Let $(Y, \text{Ker}(\alpha))$ be a contact 3-manifold with contact form α and $(\mathbb{R} \times Y, d(e^t\alpha))$ its symplectization. Let Λ_+ and Λ_- be two Legendrian links in $(Y, \text{Ker}(\alpha))$. A *Lagrangian cobordism* (with cylindrical ends) from Λ_- to Λ_+ is an embedded Lagrangian surface L satisfying:

- (1) $L \cap [-N, N] \times Y$ is compact,
- (2) $L \cap [N, \infty) \times Y \cong [N, \infty) \times \Lambda_+$,
- (3) $L \cap (-\infty, -N] \times Y \cong (-\infty, -N] \times \Lambda_-$,

for some N sufficiently large.

An *immersed Lagrangian cobordism* is defined similarly, as an immersed Lagrangian surface but with embedded cylindrical ends.

Remark 2.2. The cylindrical ends condition of the definition is equivalent to requiring that the Liouville vector field ∂_t is tangent to L in the half-cylinders $(-\infty, N] \times Y$ and $[N, \infty) \times Y$.

A priori, the cylindrical ends condition depends on the contact form α and the corresponding Liouville vector field. However, if the ends are infinite, they are cylindrical for any chosen contact form, as explained in the following lemma.

Lemma 2.3. *Suppose that L is a Lagrangian cobordism with cylindrical ends from Λ_- to Λ_+ in $(\mathbb{R} \times Y, d(e^t \alpha))$. Let $\alpha' = f\alpha$ be another contact form for $\xi = \ker(\alpha)$, where f a positive function. Then the image of L under the symplectomorphism $\Phi : (\mathbb{R} \times Y, d(e^t \alpha)) \rightarrow (\mathbb{R} \times Y, d(e^t \alpha'))$ given by the map*

$$\Phi(t, x) = (-\log(f(x)) + t, x)$$

is also a Lagrangian cobordism from Λ_- to Λ_+ with cylindrical ends.

Proof. Let $M_+ = \max_Y(-\log f)$ and $M_- = \min_Y(-\log f)$. Then

$$\Phi([-N, N] \times Y) \subset [-N + M_-, N + M_+] \times Y,$$

and furthermore

$$\begin{aligned} \Phi^{-1}([N + M_+, \infty) \times \Lambda_+) &\subset [N, \infty) \times \Lambda_+, \\ \Phi^{-1}((-\infty, -N + M_-] \times \Lambda_-) &\subset (-\infty, -N] \times \Lambda_-. \end{aligned}$$

This implies that

$$\begin{aligned} \Phi(L) \cap [N + M_+, \infty) \times Y &= [N + M_+, \infty) \times \Lambda_+, \\ \Phi(L) \cap (-\infty, -N + M_-] \times Y &= (-\infty, -N + M_-] \times \Lambda_-, \end{aligned}$$

and $\Phi(L)$ is still a Lagrangian cobordism from Λ_- to Λ_+ with cylindrical ends. \square

Lagrangian cobordisms with cylindrical ends can be glued together. We state but do not prove the following result, as it is similar to [Proposition 2.8](#) below.

Proposition 2.4. *If L_a is a Lagrangian cobordism with cylindrical ends from Λ_1 to Λ_2 and L_b is a Lagrangian cobordism with cylindrical ends from Λ_2 to Λ_3 , there is a Lagrangian cobordism from Λ_1 to Λ_3 that is the smooth, topological concatenation of L_a with L_b*

Definition 2.5. A *strong symplectic filling* of a contact structure (Y, ξ) is a compact symplectic manifold (X, ω) with $\partial X = Y$, an outward-pointing Liouville vector field ρ along Y , such that $\xi = \text{Ker}(\omega(\rho, -)|_Y)$. If (X, ω, ρ) is a strong filling, let $(\widehat{X}_\rho, \widehat{\omega})$ denote the symplectic manifold obtained by adding the half-infinite collar $[0, \infty) \times Y$ to X and extending ω as $d(e^t \omega(\rho, -))$ on the half-infinite cylinder.

A *strong symplectic cap* (X, ω, ρ) of a contact structure (Y, ξ) is defined similarly to a strong filling, except the Liouville vector field is inward-pointing along $\partial X = Y$. Let $(\widehat{X}, \widehat{\omega})$ denote the symplectic manifold obtained by adding the half-infinite cylinder $(-\infty, 0] \times Y$ to X and extending ω as $d(e^t \omega(\rho, -))$ on the half-infinite cylinder.

Definition 2.6. Let (Y, ξ) be a contact manifold and L a Legendrian link in (Y, ξ) . A *Lagrangian filling* of L in a strong symplectic filling (X, ω, ρ) of (Y, ξ) is a Lagrangian submanifold $\Lambda \subset (\widehat{X}_\rho, \widehat{\omega})$ such that

$$\Lambda \cap [N, \infty) \times Y = [N, \infty) \times L$$

for N sufficiently large.

A *Lagrangian cap* in a strong symplectic cap is a Lagrangian submanifold $\Lambda \subset (\widehat{X}, \widehat{\omega})$ such that

$$\Lambda \cap (-\infty, -N] \times Y = (-\infty, -N] \times L$$

for N sufficiently large.

An *immersed Lagrangian filling/cap* is defined similarly, as an immersed Lagrangian surface but with embedded cylindrical ends.

Remark 2.7. As in [Definition 2.1](#), the definition of cylindrical ends depends on the choice of contact form α and associated Liouville vector field. But as in [Lemma 2.3](#), the *existence* of cylindrical ends is independent of the contact form.

The key gluing result is that a Lagrangian filling and a Lagrangian cap can be glued together to obtain a closed Lagrangian surface in a closed symplectic 4-manifold.

Proposition 2.8 (Gluing). *Let (Y, ξ) be a contact 3-manifold and $\Lambda \subset (Y, \xi)$ a Legendrian link. Suppose that*

- (1) (X_f, ω_f) is a strong symplectic filling of (Y, ξ) and L_f is a Lagrangian filling of Λ in (X_f, ω_f) ,
and
- (2) (X_c, ω_c) is a strong symplectic cap of (Y, ξ) and L_c is a Lagrangian cap of Λ in (X_c, ω_c) .

Then, after possibly rescaling ω_f ,

- (1) the symplectic cap and filling can be glued to obtain a closed, symplectic 4-manifold (X, ω) ,
and
- (2) the Lagrangian cap and filling can be glued to obtain a closed, Lagrangian surface $L \subset (X, \omega)$.

Proof. Let ρ_f be the outward-pointing Liouville vector field for (X_f, ω_f) and ρ_c the inward-pointing Liouville vector field for (X_c, ω_c) . Given a contactomorphism $\Phi : \partial X_f \rightarrow \partial X_c$ sending Λ to Λ , we can identify the induced contact forms, up to multiplying by a positive function:

$$\alpha_f = \omega_f(\rho_f, -) = g\omega_c(\rho_c, -) = g\Phi^*(\alpha_c).$$

Let N_f, N_c be sufficiently large constants guaranteeing cylindrical ends for L_f, L_c , respectively. Then, as in [Lemma 2.3](#) and after possibly scaling ω_f by some small constant C , we can extend Φ to a symplectic embedding

$$\Phi : [N_f, 2N_f] \times Y \subset (\widehat{X}_f, C\widehat{\omega}_f) \hookrightarrow (-\infty, -N_c] \times Y \subset (\widehat{X}_c, \widehat{\omega}_c).$$

This identifies the Lagrangian cylinders over Λ as well. The closed symplectic manifold (X, ω) can be constructed as the union of the sublevel set of $\left\{\frac{3}{2}N_f\right\} \times Y$ in $(\widehat{X}_f, C\widehat{\omega}_f)$ and the superlevel set of $\Phi\left(\left\{\frac{3}{2}N_f\right\} \times Y\right)$ in $(\widehat{X}_c, \widehat{\omega}_c)$. \square

2.2. Filling the unlink.

Proposition 2.9. *Let \mathcal{U}_n be an n -component Legendrian unlink in (S^3, ξ_{std}) such that every component has $tb = -1$. Let $W = (B^4, \omega, \rho)$ be a Liouville filling of (S^3, ξ_{std}) . Then \mathcal{U}_n has a Lagrangian filling by disjoint Lagrangian disks in W .*

Proof. Let $\Lambda \subset (S^3, \xi_{std} = \ker \alpha)$ be a standard Legendrian unlink Λ of n Legendrian unknots with $tb = -1$, meaning that the front projection of Λ consists of n components in disjoint disks, each with no crossings and exactly two cusps.

See [\[Bla+21\]](#) for a survey of standard constructions of Lagrangian cobordisms. In particular, Theorem 2 in [\[Bla+21\]](#), attributed to [\[BST15\]](#) and [\[EHK16\]](#), implies that Λ has a filling by disjoint Lagrangian disks in the negative symplectization $((-\infty, 0] \times S^3, d(e^t\alpha))$. By the classification of Legendrian unlinks [\[EF98\]](#), this Λ is Legendrian isotopic to \mathcal{U}_n . It follows from [\[Cha10\]](#) that there is a Lagrangian concordance from \mathcal{U}_n to Λ , which can be glued to our filling of Λ to get a filling of \mathcal{U}_n in $((-\infty, 0] \times S^3, d(e^t\alpha))$.

Now note that flowing inward along the Liouville vector field ρ from the boundary of (B^4, ω, ρ) gives a symplectic embedding of $((-\infty, 0] \times S^3, d(e^t\alpha))$ into (B^4, ω, ρ) , and thus gives a Lagrangian filling of \mathcal{U}_n in (B^4, ω, ρ) . \square

2.3. Filling general links by immersed Lagrangian surfaces. We next generalize to the case of arbitrary Legendrian links. Here we will explain that the h -principle for formal Legendrian embeddings implies that a Legendrian link admits a filling by immersed Lagrangian disks if and only if each component has vanishing rotation number.

The contact structure (S^3, ξ_{std}) admits a global, nonvanishing section τ since the Euler class of ξ_{std} vanishes. In addition, since $H^1(S^3; \mathbb{Z}) = 0$, this section is unique up to homotopy. Let Λ be an immersed Legendrian curve, which we view as a map

$$\Lambda : S^1 \rightarrow S^3.$$

Consider the pullback bundle $\Lambda^*(\xi)$ over S^1 . Let v be a nonvanishing vector field along S^1 that points in the positive direction. Since Λ is Legendrian, the image $d\Lambda(v)$ is a nonvanishing section of ξ , which pulls back to give a nonvanishing section of $\Lambda^*(\xi)$, which by abuse of notation we also denote by v . In addition, the global section τ pulls back to give a section of $\Lambda^*(\xi)$. The obstruction class $d^1(v, \tau)$ to homotoping v to τ through nonvanishing sections is an element of $H^1(S^1, \mathbb{Z}) \cong \mathbb{Z}$. This integer is called the *rotation number* of the Legendrian immersion Λ and is denoted $\text{rot}(\Lambda)$.

The h -principle for formal Legendrian immersions (see [EM02]) implies that the rotation number is a complete invariant up to Legendrian homotopy.

Proposition 2.10. *Let Λ_0, Λ_1 be two n -component Legendrian links. There exists a family Λ_t of immersed Legendrian links for $t \in [0, 1]$ connecting Λ_0 to Λ_1 if and only if for all $i = 1, \dots, n$*

$$\text{rot}(\Lambda_{0,i}) = \text{rot}(\Lambda_{1,i})$$

where $\Lambda_{k,i}$ denotes the i^{th} -component of the link Λ_k .

Lemma 2.11. *If there exists a Legendrian homotopy from Λ to Λ' , then there exists an immersed Lagrangian concordance of from Λ to Λ' .*

Moreover, if the Legendrian homotopy from Λ to Λ' consists of p positive crossing changes and n negative crossing changes, the Lagrangian concordance has p positive and n negative transverse self-intersections.

Proof. We can decompose a Legendrian homotopy L_t into a sequence of isotopies and crossing changes. Each of these correspond to a Lagrangian cobordism with cylindrical ends, which can be concatenated to produce the immersed Lagrangian filling. The case of a Legendrian isotopy is covered by [Cha10] and we describe the case of the crossing change by the following local model.

Choose Darboux coordinates (s, x, y, z) such that

$$\alpha = dz - ydx \quad d(e^s \alpha) = e^s (ds \wedge (dz - ydx) + dx \wedge dy).$$

Consider the following surfaces, parameterized by $(a, b) \in \mathbb{R}^2$:

$$L_1 = (a, 0, b, 0) \quad L_2 = (a, b, 0, \phi_\epsilon(a))$$

where ϕ_ϵ is a smooth step function that equals $-\epsilon$ for $a \leq -\epsilon$ and equals ϵ for $a \geq \epsilon$. These surfaces can be immediately checked to be Lagrangian with respect to $\omega = d(e^s(\alpha))$ and have cylindrical ends with respect to the Liouville vector field ∂_s . Furthermore, the intersection of $L_1 \cup L_2$ as a varies from $-\epsilon$ to ϵ traces a Legendrian homotopy through a crossing change. Replacing ϕ_ϵ by $-\phi_\epsilon$ changes the sign of the crossing change. \square

Proposition 2.12. *Let Λ be an n -component Legendrian link in (S^3, ξ_{std}) such that every component has $\text{rot} = 0$. Let $W = (B^4, \omega, \rho)$ be a Liouville filling of (S^3, ω_{std}) . Then Λ has a Lagrangian filling by immersed Lagrangian disks in W .*

Proof. By [Proposition 2.10](#), the link Λ is Legendrian homotopic to the maximal unlink \mathcal{U}_n , where each component has $tb = -1$ and $\text{rot} = 0$. This latter link has a Lagrangian filling by embedded disks. Furthermore, by [Lemma 2.11](#), the trace of the Legendrian homotopy from \mathcal{U}_n to Λ can be realized by an immersed Lagrangian cylinder. This can be glued to the Lagrangian filling of \mathcal{U}_n to produce an immersed Lagrangian filling of Λ . \square

3. CONSTRUCTING LAGRANGIAN CAPS

The goal of this section is to prove [Theorem 1.3](#), that is, to show how to construct a Lagrangian triple cap from a (geometric) triple grid diagram. In [Section 3.1](#) we first construct Legendrian arcs in each of the three handlebodies which connect the points on the torus given by the triple grid diagram. Then in [Section 3.2](#) we show how to put two of these solid tori together to create Legendrian links in S^3 , describe front projections of these links, and use the projections to show that these Legendrians are isotopic to those produced by the standard Legendrianization of a grid diagram as described in the introduction. Finally in [Section 3.3](#) we construct the triple cap with boundary conditions given by these Legendrian arcs.

3.1. From points on a torus to arcs in a solid torus. First we will work in an abstract solid torus $H = D^2 \times S^1$ with boundary $\Sigma = \partial H = S^1 \times S^1$. We will use coordinates (p, μ, λ) on H where $p = r^2 \in [0, 1]$ and (r, μ) are standard polar coordinates on D^2 , and λ is the angular coordinate on $S^1 = \mathbb{R}/2\pi\mathbb{Z}$. Let \mathcal{F} be the foliation of H by meridional disks, that is, disks tangent to the integrable plane field $\ker d\lambda$, and let ξ be the positive contact structure $\ker(d\lambda + pd\mu)$ on H .

Our goal, given points on Σ coming from a triple grid diagram, is to construct two sets of arcs in H connecting the points: *flat arcs* and *Legendrian arcs*. The flat arcs will be tangent to \mathcal{F} , and from these we will construct Legendrian arcs tangent to ξ . Note that a Legendrian arc in (H, ξ) is completely determined by its *front projection* onto Σ . Furthermore, the λ/μ slope of this front projection is constrained to lie between 0 and -1 , and the p coordinate is recovered from the front projection by the equation $p = -d\lambda/d\mu$ (in other words, p is the negative of the λ/μ slope).

We start with a collection of points $P_1, P'_1, \dots, P_b, P'_b$ on Σ such that each pair P_i and P'_i lie on the boundary of the same meridional disk, i.e. have the same λ coordinate. In (p, μ, λ) coordinates, these points have coordinates of the form $P_i = (1, m_i, l_i)$ and $P'_i = (1, m'_i, l_i)$. For each such pair, let D_i be the meridional disk (leaf of \mathcal{F}) $\{\lambda = l_i\}$, and choose an arc A_i in H satisfying the following four properties.

- (1) A_i is properly embedded in D_i with endpoints P_i and P'_i .
- (2) A_i does not pass through the center of the disk D_i .
- (3) A_i cuts D_i into two components, and the area of the component not containing the center $\{0\}$ of the disk (measured by the area form $dp \wedge d\mu = 2rdrd\theta$) is equal to the distance on the boundary of the disk between P_i and P'_i (measured by $d\mu$, and where we measure the distance using an arc in ∂D_i which is homotopic to A_i in $D_i \setminus \{0\}$).
- (4) On $\{p \in [1/2, 1]\}$, the arc A_i is radial, i.e. has constant angular coordinate μ .

Two such arcs and the (p, μ, λ) coordinate system on a solid torus are illustrated in [Figure 5](#).

These conditions mean that we can parameterize A_i as $(p(t), \mu(t), \lambda(t))$, with $t \in [-1, 1]$, satisfying the following conditions:

- $\lambda(t) = l_i$,
- $p(t) \in (0, 1]$,
- for $t \in [-1, -1/2]$, $p(t) = -t$ and $\mu(t) = m_i$,
- for $t \in [1/2, 1]$, $p(t) = t$ and $\mu(t) = m'_i$,

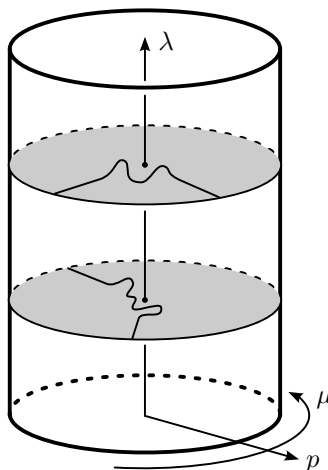


FIGURE 5. Arcs on meridional disks in a solid torus H , with radial coordinate p , meridional coordinate μ and longitudinal coordinate λ . The torus is illustrated as a cylinder, with the understanding that the top is glued to the bottom by the identity.

- and $\int_{-1}^1 p(t)\mu'(t)dt = 0$.

Now extend the domain of this parameterized curve to $t \in \mathbb{R}$ as follows:

- $\lambda(t) = l_i$ for all $t \in \mathbb{R}$,
- for $t \in [-\infty, -1/2]$, $p(t) = -t$ and $\mu(t) = m_i$,
- and for $t \in [1/2, \infty]$, $p(t) = t$ and $\mu(t) = m'_i$.

This is a parameterized curve in $\mathbb{R}^2 \times S^1$ which restricts to $D^2 \times S^1$ as the original arc in H . Then, define a new function

$$\tilde{\lambda}(t) = l_i - \int_{-1}^t p(\tau)\mu'(\tau)d\tau$$

and consider the path \tilde{A}_i parameterized by $(p(t), \mu(t), \tilde{\lambda}(t))$. This path enjoys two key properties. First, $\tilde{\lambda}'(t) = -p(t)\mu'(t)$, so that \tilde{A}_i is Legendrian with respect to the contact structure $\xi = \ker(d\lambda + pd\mu)$. Second, $\tilde{\lambda}(t) = l_i$ for $t \in (-\infty, -1/2] \cup [1/2, \infty)$, so that \tilde{A}_i agrees with A_i for $p \geq 1/2$. This fact is straightforward for $t \in (-\infty, -1/2]$ but depends on the enclosed area condition to get the result for $t \in [1/2, \infty)$.

Note that the flat arcs A_i can be recovered from the Legendrian arcs \tilde{A}_i simply by projecting onto the appropriate meridional disks, and that in fact this projection is the standard Lagrangian projection of a Legendrian. Although the above discussion describes the Legendrian arcs as constructed from the flat arcs, in fact in the proof of the following proposition we will construct the Legendrian arcs first and then get the flat arcs as their Lagrangian projections. Some care is needed in constructing the Legendrian arcs to make sure that their Lagrangian projections are in fact embedded.

Proposition 3.1. *Given the initial data of b pairs of points $P_i = (1, m_i, l_i)$ and $P'_i = (1, m'_i, l_i)$ on Σ , with $m_i < m'_i$, and given some $\epsilon > 0$ such that the b intervals $[l_i - \epsilon, l_i + \epsilon]$ are disjoint, there exists a system of flat arcs A_i and corresponding Legendrian arcs \tilde{A}_i related as above with the following properties.*

- (1) Each \tilde{A}_i lies in the 3-dimensional wedge $\{(p, \mu, \lambda) \mid m_i - \epsilon < \mu < m_i + \epsilon, l_i - \epsilon \leq \lambda \leq l_i + \epsilon\}$.

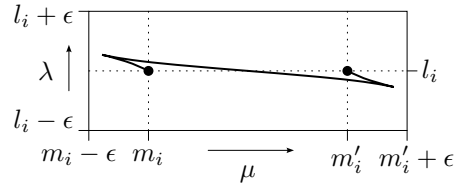


FIGURE 6. Front projection of a Legendrian arc in a solid torus, with all slopes between 0 and $-1/2$.

- (2) The front projection of each \tilde{A}_i has the qualitative features illustrated in Figure 6, i.e. starts at P_i , heads up and to the left, encounters a cusp, then turns down and to the right, passes P'_i on the left, encounters another cusp, and then turns up and to the left to end up at P'_i .

Furthermore, any two such choices of systems of flat arcs A_i (flat b -component tangles) yield systems of Legendrian arcs \tilde{A}_i (Legendrian b -component tangles) which are Legendrian isotopic rel. $\{1/2 \leq p \leq 1\}$.

Proof. The fact that any two Legendrian arcs with front projections as in Figure 6 are Legendrian isotopic simply follows from the fact that the qualitative features described determine the planar isotopy type of the front diagram, and we can easily arrange to keep the slopes between 0 and $-1/2$ so that the arcs are radial for $p \in [1/2, 1]$. Another feature of the front diagram is that the slope can be arranged to be monotonically increasing for the first half of the path from P_i to P'_i , and then monotonically decreasing for the second half of the path. This means that the Lagrangian projection to the (p, μ) coordinate plane is embedded, and it is precisely this Lagrangian projection, when placed in the meridional disk at $\lambda = l_i$, that is the flat arc A_i . If we are not careful about the slopes we may not get embedded flat arcs. \square

Definition 3.2. A system of flat arcs $\{A_i\}$ and associated system of Legendrian lifts \tilde{A}_i as in Proposition 3.1 will be called a *trivial flat tangle* with associated *trivial Legendrian tangle*.

3.2. Putting two solid tori together. We now consider S^3 built by gluing two solid tori H_α and H_β together, each a copy of the standard solid torus H discussed in the preceding section, now with coordinates $(p_\alpha, \mu_\alpha, \lambda_\alpha)$ and $(p_\beta, \mu_\beta, \lambda_\beta)$. In the standard Heegaard splitting, we see S^3 as $H_\alpha \cup H_\beta$ where the coordinates on $\Sigma_\alpha = \partial H_\alpha$ and $\Sigma_\beta = \partial H_\beta$ are related by the (orientation reversing) identifications:

$$\begin{aligned}\mu_\beta &= \lambda_\alpha, \\ \lambda_\beta &= \mu_\alpha.\end{aligned}$$

The two contact structures ξ_α and ξ_β coming from the contact structure ξ on H then glue together to give the standard contact structure on S^3 .

Now, given a collection of $2b$ points on the torus $\Sigma_\alpha = \Sigma_\beta$ forming, in the μ_α direction, pairs with the same λ_α coordinates and, in the $\mu_\beta = \lambda_\alpha$ direction, pairs with the same $\lambda_\beta = \mu_\alpha$ coordinates, we can construct trivial flat tangles and associated trivial Legendrian tangles in each solid torus H_α and H_β . Since the Legendrian tangles are radial near the boundary of each solid torus, they glue together to form a closed Legendrian link in $(S^3_{\alpha\beta}, \xi_{\alpha\beta})$.

Proposition 3.3. *Given a geometric triple grid diagram D , the Legendrian link constructed by gluing together the trivial Legendrian tangles coming from Proposition 3.1 in the solid tori H_α and H_β is Legendrian isotopic to the standard $\alpha\beta$ Legendrianization $\Lambda_{\alpha\beta}$ of the grid diagram. Cyclically permuting the three colors gives the same result for $\beta\gamma$ and for $\gamma\alpha$.*

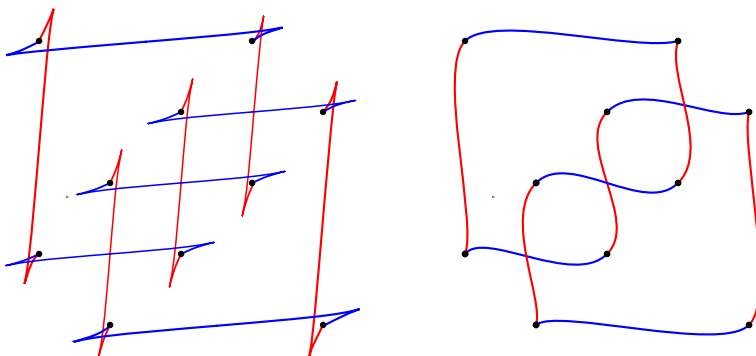


FIGURE 7. Two different front projections for a trefoil, the one on the left coming from a grid diagram via our Legendrian tangle construction and the one on the right coming from the same grid diagram via the standard Legendrianization process.

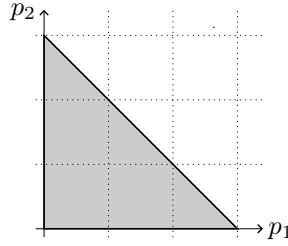
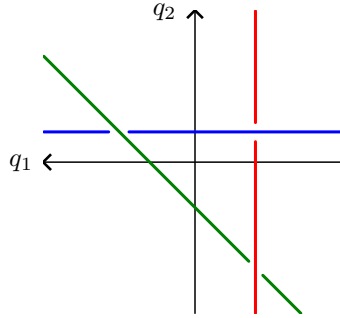
Proof. The Legendrian produced by gluing together our Legendrian tangles has a front projection obtained from the grid diagram by replacing each vertical and horizontal arc by a vertical or horizontal copy of the front diagram shown in Figure 6. Figure 7 compares the resulting front diagram for a simple grid diagram of the trefoil to the front diagram coming from the standard Legendrianization. Note that to implant the local front diagram in Figure 6 into Figure 7, we need to remember that, when the boundary of the H_α solid torus is identified with the torus on which the $\alpha\beta$ grid diagram is drawn, the μ axis points up and the λ axis points left, while with respect to the H_β solid torus, the μ axis points to the left and the λ axis points up. In other words, red is a copy of Figure 6 rotated counterclockwise 90° while blue is a copy of Figure 6 reflected across the vertical axis. The two fronts illustrated are related by Legendrian Reidemeister I and Reidemeister II moves, and this example is sufficient to illustrate the general case. \square

3.3. Constructing the triple cap. We first establish standard toric coordinates on $\mathbb{C}\mathbb{P}^2$ so that we can work with $\mathbb{C}\mathbb{P}^2$ via its moment map image. Starting with homogeneous coordinates $[z_1 : z_2 : z_3]$ on $\mathbb{C}\mathbb{P}^2$, consider standard (scaled) toric coordinates:

$$\begin{aligned} p_1 &= \frac{3|z_1|^2}{|z_1|^2 + |z_2|^2 + |z_3|^2} \in [0, 3], \\ q_1 &= \arg(z_1/z_3) \in \mathbb{R}/2\pi\mathbb{Z}, \\ p_2 &= \frac{3|z_2|^2}{|z_1|^2 + |z_2|^2 + |z_3|^2} \in [0, 3], \\ q_2 &= \arg(z_2/z_3) \in \mathbb{R}/2\pi\mathbb{Z}. \end{aligned}$$

The standard moment map is the map $\Pi : \mathbb{C}\mathbb{P}^2 \rightarrow \Delta$ given by $\Pi([z_1 : z_2 : z_3]) = (p_1, p_2)$, where Δ is the right triangle in \mathbb{R}^2 with vertices at $(0, 0)$, $(0, 3)$ and $(3, 0)$. This is illustrated in Figure 8. With respect to these coordinates, the standard symplectic structure on $\mathbb{C}\mathbb{P}^2$ (up to scale) is $\omega = dp_1 \wedge dq_1 + dp_2 \wedge dq_2$.

We henceforth view our triple grid diagram D as living on the torus $\Sigma = \Pi^{-1}(1, 1)$ with coordinates (q_2, q_1) , where this orientation is chosen so that the product coordinates $(p_1, p_2) \times (q_2, q_1)$ on $\Delta \times \Sigma$ give the same orientation as our correctly oriented toric coordinates (p_1, q_1, p_2, q_2) on $\mathbb{C}\mathbb{P}^2$. However, we draw the q_2 axis vertical and oriented upwards and the q_1 axis horizontal and oriented to the left. (We know this is confusing but ask the reader to bear with us, it is worth the time to get

FIGURE 8. Moment map image for $\mathbb{C}\mathbb{P}^2$.FIGURE 9. The (q_2, q_1) -plane.

orientation conventions correct.) The horizontal lines in our grid are thus parallel to the q_1 -axis, or given by the level sets of the function q_2 , the vertical lines are parallel to the q_2 -axis, or given by the level sets of the function q_1 , and the diagonal lines, which we have been calling the “slope -1 diagonals”, are given by the level sets of $q_1 - q_2$. This is illustrated in [Figure 9](#).

The standard trisection of $\mathbb{C}\mathbb{P}^2 = X = X_1 \cup X_2 \cup X_3$ is explicitly described as:

$$X_1 = \{(p_1, q_1, p_2, q_2) \mid p_1 + 2p_2 \leq 3, 2p_1 + p_2 \leq 3\},$$

$$X_2 = \{(p_1, q_1, p_2, q_2) \mid p_1 + 2p_2 \geq 3, p_1 \leq p_2\},$$

$$X_3 = \{(p_1, q_1, p_2, q_2) \mid 2p_1 + p_2 \geq 3, p_1 \geq p_2\}.$$

The pairwise intersections are the solid handlebodies (solid tori) $H_{ij} = X_i \cap X_j$; a more conventional trisector’s labelling is $H_\alpha = H_{31}$, $H_\beta = H_{12}$, $H_\gamma = H_{23}$. The boundary of each of these solid tori is the central genus one surface Σ . The core circles of the solid tori are given in coordinates as follows:

$$C_\alpha = \{(p_1, q_1, p_2, q_2) \mid (p_1, p_2) = (3/2, 0)\} \subset H_\alpha,$$

$$C_\beta = \{(p_1, q_1, p_2, q_2) \mid (p_1, p_2) = (0, 3/2)\} \subset H_\beta,$$

$$C_\gamma = \{(p_1, q_1, p_2, q_2) \mid (p_1, p_2) = (3/2, 3/2)\} \subset H_\gamma.$$

(Since the (p_1, p_2) points $(3/2, 0)$, $(0, 3/2)$ and $(3/2, 3/2)$ are in the interiors of edges of Δ , the (q_1, q_2) torus is collapsed to a circle in each case.) This is all illustrated in [Figure 10](#).

Although our overall construction is naturally associated with a trisection of $\mathbb{C}\mathbb{P}^2$, in which Σ is the central surface, we will in fact see that to give the construction as explicitly as possible it will be useful to decompose $\mathbb{C}\mathbb{P}^2$ into many more than three pieces. It is important to note, however, that our entire construction will be invariant under the order 3 cyclic permutation $[z_1 : z_2 : z_3] \mapsto [z_2 : z_3 : z_1] \mapsto [z_3 : z_1 : z_2] \mapsto [z_1 : z_2 : z_3]$, which also cyclically permutes the vertices of Δ and induces the order 3 cyclic permutation of our grid diagram. We will exploit this so that in some sense we only give one third of the construction and then apply this cyclic permutation.

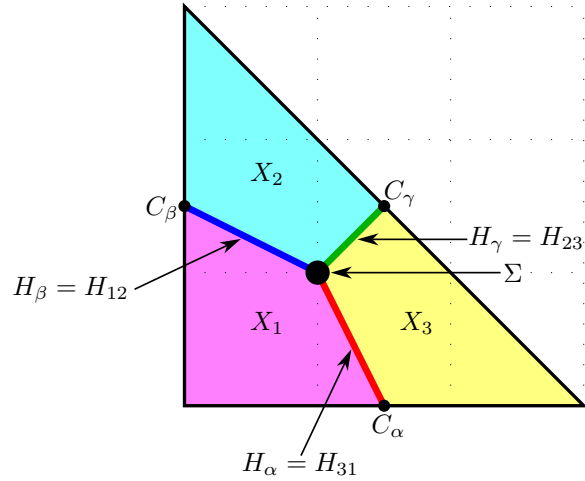


FIGURE 10. The standard trisection seen via the moment map.

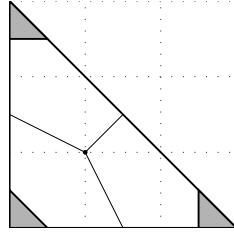


FIGURE 11. The images of three balls under the moment map, along with the trisection for reference.

First we note that the three 4-balls defined in the introduction are given in toric coordinates as:

$$B_1 = \{p_1 + p_2 \leq 1/2\}$$

$$B_2 = \{3 - p_2 \leq 1/2\}$$

$$B_2 = \{3 - p_1 \leq 1/2\}$$

These are illustrated in [Figure 11](#), which thus also illustrates our 4-manifold with three boundary components, X , via its moment map image, which is a hexagon obtained by cutting three small corners off of the right triangle Δ . The three inward-pointing Liouville vector fields appear in the moment map image as the three radial vector fields emanating from the corners of Δ , and are given in coordinates as:

$$V_1 = p_1 \partial_{p_1} + p_2 \partial_{p_2},$$

$$V_2 = p_1 \partial_{p_1} + (p_2 - 3) \partial_{p_2},$$

$$V_3 = (p_1 - 3) \partial_{p_1} + p_2 \partial_{p_2}.$$

We will also want to work with the *symplectic vector fields* $S_{ij} = (1/3)(V_i - V_j)$. (The factor of $1/3$ is just for convenience in coordinate expressions.) In certain regions the Lagrangians we construct will be tangent to, and invariant under flow along, one or more of these symplectic vector fields. For

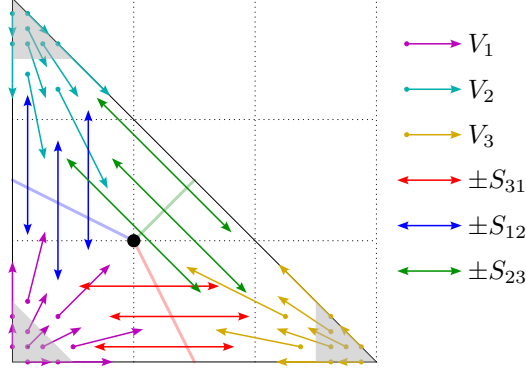


FIGURE 12. Three Liouville and three symplectic vector fields.

future reference we give them in coordinates here:

$$\begin{aligned} S_{13} &= \partial_{p_1} = -S_{31}, \\ S_{12} &= \partial_{p_2} = -S_{21}, \\ S_{23} &= \partial_{p_1} - \partial_{p_2} = -S_{32}. \end{aligned}$$

These vector fields are illustrated in [Figure 12](#).

We have already established an orientation on Σ , namely by the ordered coordinates (q_2, q_1) . We will orient each solid torus H_\bullet so that $\partial H_\bullet = \Sigma$ as oriented manifolds. Define the following “ p -coordinate” on each H_\bullet :

$$\begin{aligned} p_\alpha &= p_2, \\ p_\beta &= p_1, \\ p_\gamma &= 3 - p_1 - p_2. \end{aligned}$$

Then each solid torus minus its core, $H_\bullet \setminus C_\bullet$, is explicitly parameterized, respecting orientations, as $(0, 1] \times T^2$ by the coordinates (p_\bullet, q_2, q_1) .

Note that the symplectic vector field S_{13} is transverse to H_α , S_{12} is transverse to H_β and S_{23} is transverse to H_γ . Thus each induces a closed 1-form $\eta_\bullet = \iota_{S_{ij}} \omega|_{H_\bullet}$, and any Lagrangian surface which is tangent to S_{ij} must intersect the corresponding solid torus H_\bullet in curves which are tangent to the kernel of η_\bullet . These 1-forms are as follows, expressed in the coordinates (p_\bullet, q_2, q_1) :

$$\begin{aligned} \eta_\alpha &= dq_1, \\ \eta_\beta &= dq_2, \\ \eta_\gamma &= dq_1 - dq_2. \end{aligned}$$

The kernels of these closed 1-forms integrate to give foliations of the handlebodies by meridional disks; we label these foliations \mathcal{F}_α , \mathcal{F}_β and \mathcal{F}_γ .

In fact we can do more to standardize coordinates on our handlebodies: If p_\bullet is a radial coordinate on the solid torus H_\bullet , then we can also write down meridional and longitudinal coordinates μ_\bullet and λ_\bullet as follows:

$$\begin{aligned} \mu_\alpha &= q_2, \lambda_\alpha = q_1, \\ \mu_\beta &= q_1 - q_2, \lambda_\beta = -q_2, \\ \mu_\gamma &= -q_1, \lambda_\gamma = q_2 - q_1. \end{aligned}$$

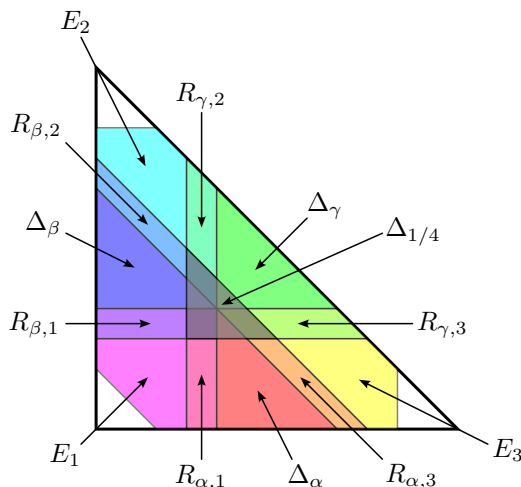


FIGURE 13. Various labelled parts of the moment image of $\mathbb{C}\mathbb{P}^2$, corresponding to steps in the construction of our Lagrangian triple cap.

In other words, the coordinates $(p_\bullet, \mu_\bullet, \lambda_\bullet)$ explicitly parameterize H_\bullet as $D^2 \times S^1$ via $(p_\bullet, \mu_\bullet) = (r^2, \theta)$ giving polar coordinates (r, θ) on D^2 and λ_\bullet being the angular coordinate on the S^1 factor. Each foliation \mathcal{F}_\bullet is then just given by parallel meridional disks $D^2 \times \{c\}$ for $c \in S^1$, and is tangent to the kernel of the closed 1-form $d\lambda_\bullet$. For the record, note that the symplectic form ω restricts to each meridional disk as the area form $dp_\bullet \wedge d\mu_\bullet = 2rdrd\theta$ which is *twice* the standard area form on D^2 .

Proof of Theorem 1.3. Our Lagrangian cap will be constructed so as to be invariant under the symplectic vector fields S_{ij} in neighborhoods of the solid tori H_\bullet , so we begin the construction by applying the methods of Section 3.1 to turn a given geometric triple grid diagram into a system of flat arcs and associated system of Legendrian lifts in each solid torus H_α , H_β and H_γ , as in Proposition 3.1. First we work with the system A_i of flat arcs and \tilde{A}_i of Legendrian lifts in H_α and we begin building our Lagrangian surface $L(D)$ in pieces, with agreement on the overlaps so as to ensure smoothness.

Let $\Delta_{1/4} \subset \Delta$ be the right triangle in the (p_1, p_2) -plane with vertices at $(3/4, 3/4)$, $(3/4, 3/2)$ and $(3/2, 3/4)$ as indicated in the center of Figure 13 (the grey triangle). Let $P \subset \Sigma$ be the set of points making up our diagram D . Recall that $\Pi : \mathbb{C}\mathbb{P}^2 \rightarrow \Delta$ is our moment map. In $\Pi^{-1}(\Delta_{1/4}) \subset \mathbb{C}\mathbb{P}^2$, note that our toric coordinates (p_1, p_2, q_2, q_1) parameterize $\Pi^{-1}(\Delta_{1/4})$ as $\Delta_{1/4} \times \Sigma$. With respect to this parameterization, let $L(D) \cap \Pi^{-1}(\Delta_{1/4}) = \Delta_{1/4} \times P$; this is just one “flat” copy of $\Delta_{1/4}$ for each point on the grid diagram, and is clearly Lagrangian.

Now let $\Delta_\alpha \subset \Delta$ be the right triangle with vertices at $(1, 0)$, $(1, 1)$ and $(2, 0)$, shown in Figure 13 as the red triangle at the bottom. Note that $H_\alpha \subset \Pi^{-1}(\Delta_\alpha)$ and that flow forwards and backwards along the symplectic vector field S_{13} starting at H_α sweeps out all of $\Pi^{-1}(\Delta_\alpha)$. Let $F(D) \cap \Pi^{-1}(\Delta_\alpha)$ be the surface obtained by flowing all the chosen flat arcs A_i in H_α forwards and backwards along this vector field $S_{13} = \partial_{p_1}$. As discussed above, this is Lagrangian because the arcs are tangent to the kernel of the 1-form $\iota_{S_{13}}\omega|_{H_\alpha}$. Also note that, because each arc is radial on $\{p_\alpha \in [3/4, 1]\}$, this definition of $L(D) \cap \Pi^{-1}(\Delta_\alpha)$ agrees with our previous definition of $L(D) \cap \Pi^{-1}(\Delta_{1/4})$ on their overlap in $\Pi^{-1}(\Delta_{1/4} \cap \Delta_\alpha)$. Appropriately applying the S_3 symmetry of $\mathbb{C}\mathbb{P}^2$ (permuting the homogeneous coordinates $[z_1 : z_2 : z_3]$) tells us how to repeat this process in $\Pi^{-1}(\Delta_\beta)$ and $\Pi^{-1}(\Delta_\gamma)$, where these regions are also shown in Figure 13.

Next let $R_{\alpha,1}$ be the rectangle with vertices at $(3/4, 0)$, $(1, 0)$, $(1, 1)$ and $(3/4, 1)$, shown in [Figure 13](#), to the left of Δ_α . Here we construct $L(D)$ as a union of rectangles, one for each of the chosen arcs A_i in H_α . Recall that each such arc is parameterized by $(p_\alpha(t), \mu_\alpha(t), \lambda_\alpha(t))$ satisfying conditions outlined above. Also recall that we constructed a Legendrian lift of each of these arcs, parameterized by $(p_\alpha(t), \mu_\alpha(t), \tilde{\lambda}_\alpha(t))$. Choose a function $f : [3/4, 1] \rightarrow [3/4, 1]$ satisfying the following properties, with respect to some suitably small $\epsilon > 0$:

- for $s \in [3/4, 3/4 + \epsilon]$, $f(s) = s$,
- for $s \in [1 - \epsilon, 1]$, $f(s) = 1$,
- and for all $s \in [3/4, 1]$, $f'(s) \in [0, 1 + \epsilon]$.

Using these, we construct a Lagrangian rectangle parameterized as follows:

$$\begin{aligned} p_1(s, t) &= s, \\ q_1(s, t) &= f'(s)\tilde{\lambda}_\alpha(t), \\ p_2(s, t) &= f(s)p_\alpha(t), \\ q_2(s, t) &= \mu_\alpha(t). \end{aligned}$$

Note that in order for this to be properly embedded in $\Pi^{-1}(R_{\alpha,1})$, the domain of this parameterization needs to be $\{(s, t) \mid s \in [3/4, 1], t \in [-1/f(s), 1/f(s)]\}$, which is why we extended our original parameterized arcs to allow $t \in \mathbb{R}$. The fact that this rectangle is Lagrangian follows from the fact that $\tilde{\lambda}'_\alpha(t) = -p_\alpha(t)\mu'_\alpha(t)$. This is our construction of $L(D) \cap \Pi^{-1}(R_{\alpha,1})$.

We now make several observations about this construction that can be verified by direct computation.

- (1) This construction of $L(D) \cap \Pi^{-1}(R_{\alpha,1})$ agrees with our construction of $L(D) \cap \Pi^{-1}(\Delta_{1/4})$ over the overlap $\Delta_{1/4} \cap R_{\alpha,1}$.
- (2) For $s \in [1 - \epsilon, 1]$, where $f(s) = 1$ and $f'(s) = 0$, $L(D)$ is the same as the surface we would get by flowing our given flat arcs A_i in H_α backwards along the symplectic vector field ∂_{p_1} and thus joins smoothly with the construction of $L(D) \cap \Pi^{-1}(\Delta_\alpha)$.
- (3) For $s \in [3/4, 3/4 + \epsilon]$, where $f(s) = s$ and $f'(s) = 1$, $L(D)$ is tangent to the Liouville vector field $V_1 = p_1\partial_{p_1} + p_2\partial_{p_2}$.
- (4) Consider the solid torus $H_{\alpha,1} = \{(p_1, q_1, p_2, q_2) \mid p_1 = 3/4, 0 \leq p_2 \leq 3/4\}$. Use solid torus coordinates $(p_{\alpha,1}, \mu_{\alpha,1}, \lambda_{\alpha,1})$ on $H_{\alpha,1}$ defined as follows: $p_{\alpha,1} = (4/3)p_2$, $\mu_{\alpha,1} = q_2$, $\lambda_{\alpha,1} = q_1$. With respect to these coordinates, $L(D) \cap H_{\alpha,1}$ is the collection of arcs parameterized by $p_{\alpha,1}(t) = \tilde{\lambda}_\alpha(t)$, $\mu_{\alpha,1}(t) = \mu_\alpha(t)$, $\lambda_{\alpha,1}(t) = \tilde{\lambda}_\alpha(t)$.
- (5) In particular, each component of $L(D) \cap H_{\alpha,1}$ is an exact copy of one of the corresponding Legendrian arcs \tilde{A}_i in the solid torus H_α , and is Legendrian with respect to the contact structure induced by the Liouville vector field V_1 .

Now repeat these constructions over the remaining triangles Δ_β and Δ_γ and “rectangles” $R_{\bullet,i}$. This gives our Lagrangian $L(D)$ over all of the colored regions in [Figure 13](#) except the three “ends” E_1 , E_2 and E_3 . Since $L(D)$ is tangent to the appropriate Liouville vector fields over the outer edges of the rectangles, we extend $L(D)$ over each E_i by flowing inward along the vector field V_i and this completes our construction of $L(D)$.

Now we verify that the Legendrian links at the three boundary S^3 's are in fact Legendrian isotopic to the expected Legendrians $\Lambda_{\alpha\beta}$, $\Lambda_{\beta\gamma}$ and $\Lambda_{\gamma\alpha}$. This is clear because each of these Legendrian links is obtained by gluing together two of the given Legendrian tangles, and we have seen in [Proposition 3.3](#) that these are Legendrian isotopic to the standard Legendrianizations of our three grid diagrams.

To complete the proof, having constructed our Lagrangian surface $L(D)$, we need to show that $L(D)$ is diffeomorphic to the abstract ribbon surface $R(D)$. Referring back to Figure 13, note that $L(D)$ is diffeomorphic to that part of $L(D)$ which sits over $\Delta_{1/4} \cup \Delta_\alpha \cup \Delta_\beta \cup \Delta_\gamma$, because the rest of $L(D)$ is just built by extending collars to the boundary of this much of $L(D)$. The part sitting over $\Delta_{1/4}$ is a disjoint union of oriented disks, one for each vertex of the abstract colored trivalent graph $\Gamma(D)$, as in the construction of $R(D)$ from the introduction. The orientations of these disks are inherited from the orientation of $\Delta_{1/4}$. Sitting over Δ_α we have one band for each red edge of $\Gamma(D)$, over Δ_β one band for each blue edge, and over Δ_γ one band for each green edge. These bands are clearly attached in red-blue-green order as one goes clockwise around the boundary of each of the disks, because the regions Δ_α , Δ_β and Δ_γ are attached to $\Delta_{1/4}$ in that order.

The last thing to verify is that each band is a locally orientation-reversing band, relative to the orientations of the disks. This is because each band can be parameterized as $[0, 1] \times [-1, 1]$, where the core $[0, 1] \times \{0\}$ maps under the moment map to the corresponding red, blue or green straight line segment in Figure 10, with both endpoints at the center of the moment map image, and where each $\{t\} \times [-1, 1]$ factor maps homeomorphically onto its image, which is a straight line segment transverse to the image of the cores $[0, 1] \times \{0\}$. Thus each band connects two stacked disks, one on top of the other, *without* a twist, leading to a reversal of orientation. \square

4. EXAMPLES AND APPLICATIONS

In this section we present several examples and applications. The examples mostly come in the form of combinatorial triple grid diagrams, although as noted in Section 1, a geometric triple grid diagram may be obtained immediately from a combinatorial one.

4.1. Orientability and Euler characteristic. Orientability and the Euler characteristic can be determined easily from a triple grid diagram. The following definition is formulated in the language of combinatorial grid diagrams, but with slight modifications can be reformulated for geometric triple grid diagrams.

Definition 4.1. A triple grid diagram is *orientable* if X 's and O 's can be placed consistently in all three diagrams. That is, X 's and O 's can be placed in each diagram such that each vertex is assigned an X or an O , and each row, column, and diagonal that contains vertices has exactly one X and one O . See Figure 14.

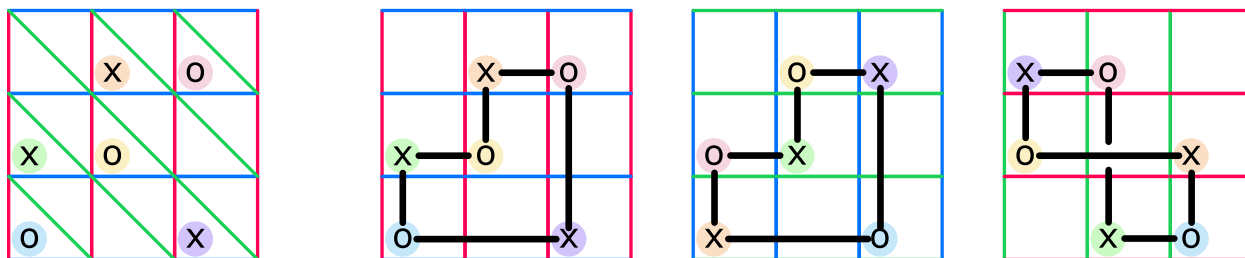


FIGURE 14. An orientable triple grid diagram. The right-hand side shows separately the three grids making up the combinatorial triple grid diagram on the left-hand side, along with the knot represented by each grid. Colors are used to indicate where each vertex in the triple grid diagram shows up in the three individual grids.

If a triple grid diagram is orientable then it determines an orientable surface, as the compatible orientations on the three knots induce an orientation on the surface. If X 's and O 's cannot be placed consistently, then the diagram determines a nonorientable surface.

Now we compute the Euler characteristic from a (combinatorial) triple grid diagram. Here we assume the surface is connected, but this calculation can be easily modified for multiple components. We will also carry out our computation for a closed surface, which we can think of as the surface obtained by abstractly filling each boundary component of the triple cap with a disk. Let b be half the number of vertices (points) of a triple grid diagram. If there are no empty rows, columns, or diagonals, then b is the same as the grid number. The Euler characteristic of the (connected) surface created from the triple grid diagram is

$$\chi = V - E + F = 2b - 3b + F = F - b,$$

where V is the number of vertices, E is the number of edges, and F is the number of faces (which is the same as the number of link components). In particular this means that for orientable surfaces $\#^g T^2$ we have

$$2 - 2g = F - b,$$

and for nonorientable surfaces $\#^k \mathbb{R}P^2$ we have

$$2 - k = F - b.$$

If we do not fill in all the boundary components with disks, the above two formulae are still correct but the Euler characteristic formula needs to be adjusted appropriately.

Note that following the work in [MZ17; MZ18; HKM20], if each of the three links in a triple grid diagram is an unlink, then we can (uniquely) construct a smoothly embedded surface by filling in these three unlinks with disks. In [Bla22], such triple grid diagrams were called *simple*. In general, these surfaces will not be Lagrangian; the additional $tb = -1$ condition that the diagram must satisfy in order to produce a closed Lagrangian surface is fairly restrictive.

There exist simple triple grid diagrams representing (smoothly) embedded $\#^g T^2$ and $\#^k \mathbb{R}P^2$ for all integers $g, k > 0$; see Example 4.6, Example 4.7, and Example 4.8. The only embedded, orientable Lagrangian surface in $\mathbb{C}P^2$ is a torus, as Lagrangians have isomorphic normal and tangent bundles. As for the nonorientable case, Shevchishin [She09] and Nemirovski [Nem09] showed that there is no Lagrangian embedding of the Klein bottle in $\mathbb{C}P^2$. Combining work of Givental [Giv86], Audin [Aud90], and Dai, Ho, and Li [DHL19], it follows that $\#^k \mathbb{R}P^2$ admits a Lagrangian embedding in $\mathbb{C}P^2$ if and only if $k \equiv 2 \pmod{4}$ for $k \neq 2$, or $k \equiv 1 \pmod{4}$. We can realize a Lagrangian $\mathbb{R}P^2$ and Lagrangian torus with small diagrams; see Example 4.3 and Example 4.4. However it remains to be seen whether all Lagrangian $\#^k \mathbb{R}P^2$'s can be realized.

Question 4.2. Can all $\#^k \mathbb{R}P^2$ for which there exists a Lagrangian embedding in $\mathbb{C}P^2$ be realized as triple grid diagrams where each link is a unlink with $tb = -1$ components?

Even though every (smoothly) embedded $\#^k \mathbb{R}P^2$ can be represented by a simple triple grid diagram, higher k values require a higher number of vertices, and it is in general very difficult to construct diagrams with many vertices without introducing unwanted cusps, which lower tb and hence makes it harder to achieve $tb = -1$.

4.2. Examples of triple grid diagrams. We now present numerous examples of (combinatorial) triple grid diagrams with various interesting properties. Each figure shows a (combinatorial) triple grid diagram, and to the right shows the three links represented by the three grids, along with the corresponding Legendrian fronts.

Example 4.3 (Grid number 2). There is one unique triple grid diagram (Figure 15) with grid number 2 and it represents an $\mathbb{R}P^2$. Each knot is an unknot, and each unknot, when viewed as the front projection of a Legendrian knot, has $tb = -1$. So the $\mathbb{R}P^2$ represented by this grid is Lagrangian.

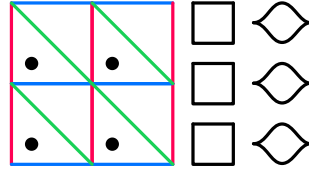


FIGURE 15. The unique triple grid diagram with grid number 2.

Example 4.4 (Grid number 3). There is one unique triple grid diagram (Figure 16) with grid number 3 and it represents a T^2 . Each knot is an unknot, and each unknot, when viewed as the front projection of a Legendrian knot, has $tb = -1$. So the T^2 represented by this grid is Lagrangian.

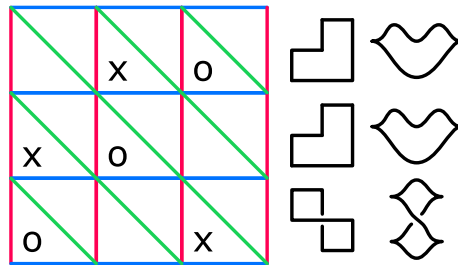


FIGURE 16. The unique triple grid diagram with grid number 3.

Example 4.5 (Another Lagrangian torus). The following diagram (Figure 17) contains a two-component unlink in one grid and unknots in the others. When we cap off with disks, we obtain a T^2 . Each of the four unknots have $tb = -1$, so this T^2 is Lagrangian.

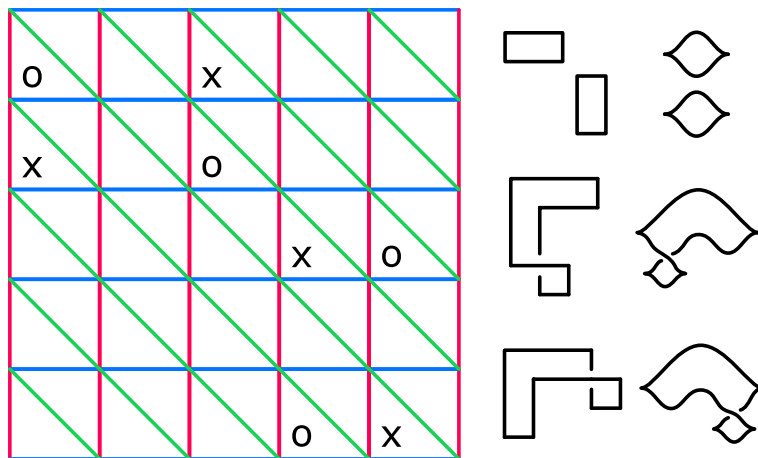


FIGURE 17. A triple grid diagram representing another Lagrangian torus.

Example 4.6 (Staircase family). Let n be the grid number. A “staircase” triple grid diagram (Figure 18), which is a diagram that looks like a staircase in one grid as shown below, produces $\mathbb{R}\mathbb{P}^2$ for even n and $\#^{\frac{n-1}{2}}T^2$ for odd n . The unknots making up the $\mathbb{R}\mathbb{P}^2$ will always have $tb = -1$, but for odd grid numbers, only $n = 3$ will produce $tb = -1$ unknots. That is, the even grids will always give closed Lagrangian surfaces, but the odd grids only give a closed Lagrangian surface for grid number 3. This is good because $n = 3$ yields a T^2 (as seen in Example 4.4), but higher n will yield a higher genus surface, and there are no other embedded, orientable Lagrangians in $\mathbb{C}\mathbb{P}^2$ besides T^2 .

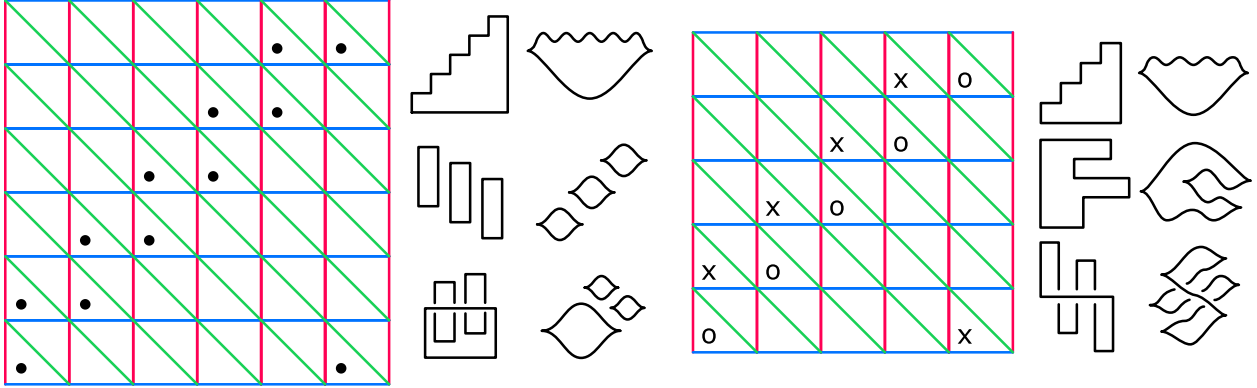


FIGURE 18. A family of “staircase” triple grid diagrams.

Example 4.7 (Klein bottle). The following diagram (Figure 19) has an unknot in each grid, some of which do not have $tb = -1$. When we fill in with disks, we obtain a $\#^2\mathbb{R}\mathbb{P}^2$ which is not Lagrangian.

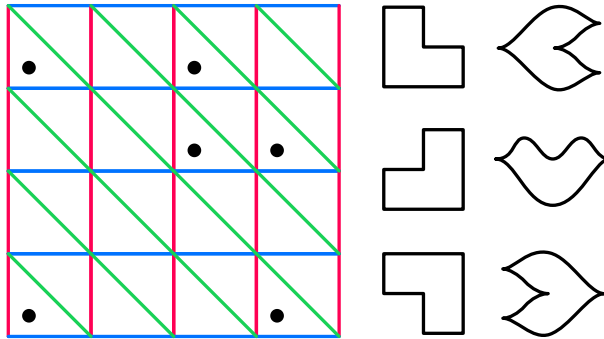


FIGURE 19. A triple grid diagram representing a Klein bottle.

Example 4.8 (Nonorientable families). The following diagrams (Figure 20) are representative of two families of diagrams which (together) produce $\#^k\mathbb{R}\mathbb{P}^2$ for all positive integers k except 2 (see Example 4.7). The left diagram, made up of k disjoint squares along the anti-diagonal, where k is odd, represents $\#^k\mathbb{R}\mathbb{P}^2$. The right diagram, made up of k disjoint squares and k disjoint “hexagons” along the anti-diagonal, where k is even, represents $\#^{k+2}\mathbb{R}\mathbb{P}^2$. Except in the case of one square, which produces $\mathbb{R}\mathbb{P}^2$ (see Example 4.3), these diagrams do not produce closed Lagrangian surfaces.

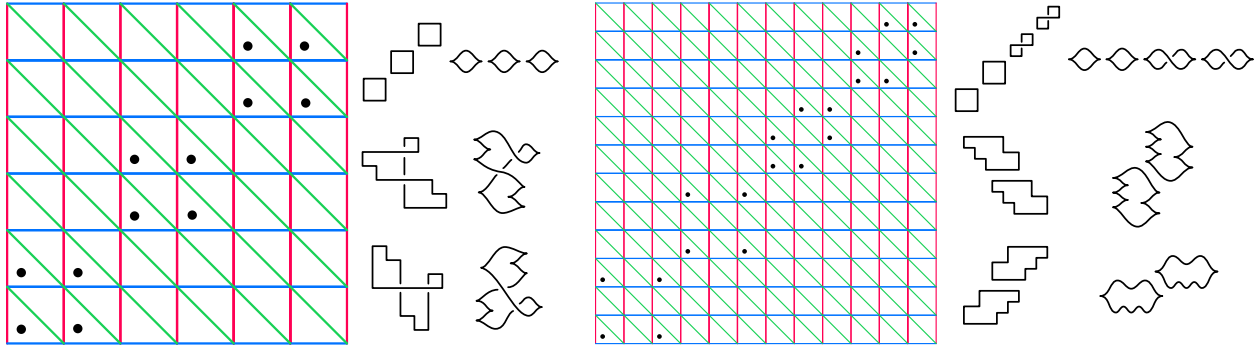


FIGURE 20. Two families of diagrams representing $\#^k \mathbb{R}P^2$ for all positive integers k except 2.

Example 4.9 (Sphere with double point). The following diagram (Figure 21) has a Hopf link in one grid and two-component unlinks in the others. If we cap off the Hopf link with two embedded disks with one intersection point, and the unlinks with embedded disks with no intersection points, we obtain a sphere with one double point which is Lagrangian by Corollary 1.6.

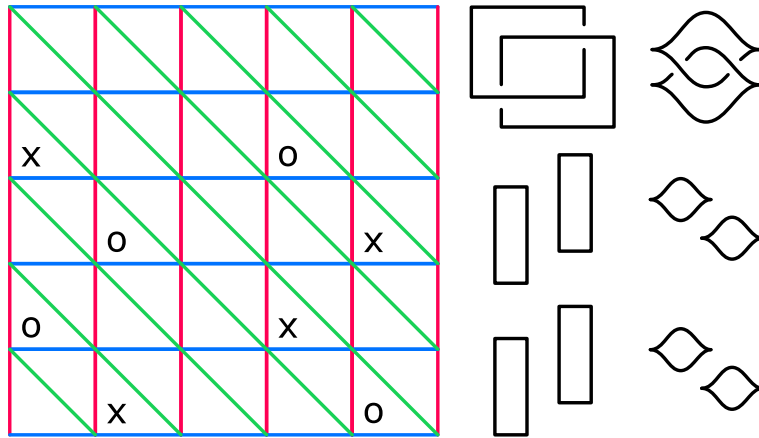


FIGURE 21. A triple grid diagram representing a sphere with a double point.

Example 4.10 (Two intersecting components). The following diagram (Figure 22) has a Hopf link in each grid. If we cap off each with two embedded disks with one intersection point, we obtain an immersed surface comprised of two embedded components which is Lagrangian by Corollary 1.6. The three Hopf links are made of $tb = -1$ unknots, so the two components are both Lagrangian $\mathbb{R}P^2$'s, and they intersect in three points.

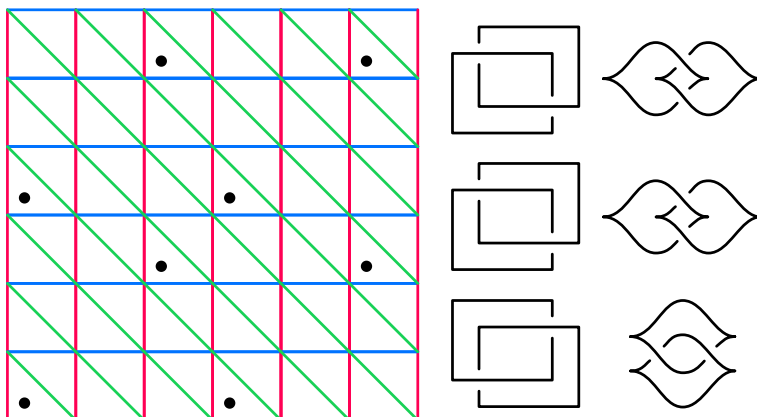


FIGURE 22. A triple grid diagram representing a surface with two intersecting components.

A general method for efficiently constructing *all* examples of triple grid diagrams has recently been introduced by Gulati and the third author [GL24].

4.3. Cap for a Legendrian and its push-off. A triple grid diagram for a cap of a Legendrian and its push-off can be constructed the following way. Start with a grid diagram for a Legendrian link, and then displace a copy of it shifted northwest by one square. Connect the vertices of the original and displaced link by diagonal lines (of slope -1). The result, after adding in crossings using our pairwise over/under conventions, is a triple grid diagram consisting of two copies of the original link along with a Legendrian unlink with $tb = -1$ components. See the diagram on the left in Figure 23. Filling in the $tb = -1$ unlink components with Lagrangian disks then creates a Lagrangian cap of the Legendrian and its push-off, which is topologically an annulus.

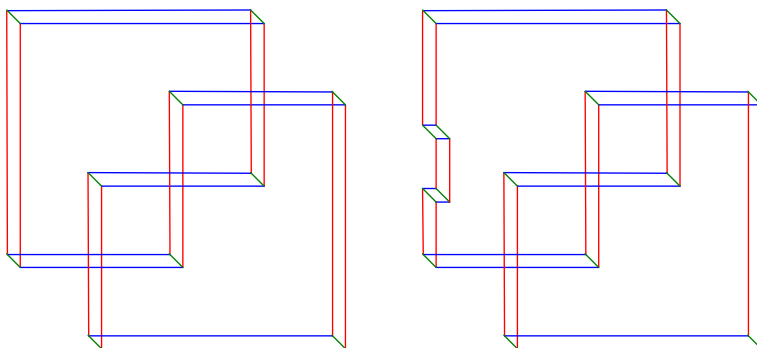


FIGURE 23. Turning a grid diagram for a trefoil into two different triple grid diagrams. On the left is a triple grid diagram that can be filled on the blue-green and green-red ends but which, on the red-blue end, is a copy of the original Legendrian and a Legendrian pushoff. On the right is a closely related fillable triple grid diagram. Note that here we have dropped the grid lines, so this can be seen as a geometric triple grid diagram and it is clear that there is a moduli space of such diagrams. In particular, as drawn there are sometimes multiple green edges in a given diagonal line, but these can be displaced by small perturbations. See [GL24] for further discussion of moduli spaces of triple grid diagrams.

From this construction we can reprove the following result:

Proposition 4.11 (Chantraine [Cha10]). *If Λ is a fillable Legendrian knot in S^3 with an orientable genus g filling and Thurston-Bennequin number $\text{tb}(\Lambda)$, then $\text{tb}(\Lambda) = 2g - 1$.*

Proof. As in the paragraph above, construct a triple grid diagram D from a grid diagram for Λ and use this to construct an annular Lagrangian cap for $\Lambda \cup \Lambda'$, where Λ' is a Legendrian pushoff of Λ . Filling Λ and Λ' by genus g Lagrangian fillings gives a closed immersed Lagrangian surface Σ of genus $2g$ with the algebraic count of double points equal to $\text{tb}(\Lambda)$. Since the algebraic intersection number $[\Sigma] \cdot [\Sigma]$ is 0, the Euler number of the normal bundle $\nu\Sigma$ is equal to $-2\text{tb}(\Lambda)$. (See, for example, Lemma 1 in [Boh02] for a statement of the standard result needed to see this.) Since Σ is Lagrangian, its normal bundle is isomorphic to its tangent bundle, so $-2\text{tb}(\Lambda) = 2 - 4g$, and thus $\text{tb}(\Lambda) = 2g - 1$. \square

The right hand diagram in Figure 23 illustrates a small change that can be made in this construction to produce a fillable triple grid diagram which always gives an embedded Lagrangian torus in $\mathbb{C}\mathbb{P}^2$. Alternatively, for any Legendrian knot Λ , the link consisting of Λ and a contact-framed push-off has an annular Lagrangian filling. Therefore, the cap and this filling can be glued to produce a closed Lagrangian torus.

4.4. Fillability obstructions. The obstructions to Lagrangian embeddings of nonorientable surfaces mentioned above can in principle obstruct Lagrangian fillings of Legendrian links. As stated, the orientability of the Lagrangian cap is determined by whether the cubic graph determined by the triple grid diagram is bipartite. In addition, the Euler characteristic of a closed surface L obtained from a triple grid diagram is determined by the formula

$$\chi(L) = c_1 + c_2 + c_3 - b$$

where c_1, c_2, c_3 are the number of components of the Legendrian links $\Lambda_{\alpha\beta}(D), \Lambda_{\beta\gamma}(D)$, and $\Lambda_{\gamma\alpha}(D)$, respectively, and $2b$ is the number of points in the grid diagram. By the classification of surfaces, this is all the information needed to determine the homeomorphism-type of the constructed surface.

Theorem 4.12. *Let D be a nonorientable triple grid diagram such that*

- (1) *the quantity $c_1 + c_2 + c_3 - b$ is equal to 0 or is strictly negative and equal to 2 or 3 (mod 4), and*
- (2) *$\Lambda_{\alpha\beta}(D)$ and $\Lambda_{\beta\gamma}(D)$ admit Lagrangian fillings by slice disks.*

Then $\Lambda_{\gamma\alpha}(D)$ does not admit a Lagrangian filling by slice disks.

Proof. Suppose, by contradiction, that $\Lambda_{\gamma\alpha}(D)$ does admit a Lagrangian filling by slice disks. Then by Corollary 1.4, we obtain a closed, embedded Lagrangian surface homeomorphic to either the Klein bottle or $\#_k \mathbb{R}\mathbb{P}^2$ for $k = 0$ or $k = 3 \pmod{4}$, which violates the embedding results of Givental [Giv86], Audin [Aud90], and Dai-Ho-Li [DHL19]. \square

This result is just the tip of the iceberg for fillability obstructions, as a triple cap for three Legendrians impose various constraints on their simultaneous fillability. We leave this as an exercise to the clever reader.

BIBLIOGRAPHY

- [Aud90] Michèle Audin. “Quelques remarques sur les surfaces lagrangiennes de Givental.” In: *Journal of Geometry and Physics* 7.4 (1990), pp. 583–598 (↑ 20, 25).
- [Bla22] Sarah Blackwell. “Combinatorial and Group Theoretic Approaches to Trisected Surfaces in 4–Manifolds.” PhD thesis. University of Georgia, 2022 (↑ 2, 3, 20).

- [Bla+21] Sarah Blackwell, Noémie Legout, Caitlin Levenson, Maÿlis Limouzineau, Ziva Myer, Yu Pan, Samantha Pezzimenti, Lara Simone Suárez, and Lisa Traynor. “Constructions of Lagrangian cobordisms.” In: *Research Directions in Symplectic and Contact Geometry and Topology*. Vol. 27. Association for Women in Mathematics Series. Springer, 2021, pp. 245–272 (↑ 8).
- [Boh02] Christian Bohr. “Immersions of surfaces in almost-complex 4-manifolds.” In: *Proceedings of the American Mathematical Society* 130.5 (2002), pp. 1523–1532 (↑ 25).
- [BST15] Frédéric Bourgeois, Joshua M. Sabloff, and Lisa Traynor. “Lagrangian cobordisms via generating families: construction and geography.” In: *Algebraic & Geometric Topology* 15.4 (2015), pp. 2439–2477 (↑ 8).
- [Cha10] Baptiste Chantraine. “Lagrangian concordance of Legendrian knots.” In: *Algebraic & Geometric Topology* 10.1 (2010), pp. 63–85 (↑ 8, 9, 25).
- [DHL19] Bo Dai, Chung-I Ho, and Tian-Jun Li. “Nonorientable Lagrangian surfaces in rational 4-manifolds.” In: *Algebraic & Geometric Topology* 19.6 (2019), pp. 2837–2854 (↑ 20, 25).
- [EHK16] Tobias Ekholm, Ko Honda, and Tamás Kálmán. “Legendrian knots and exact Lagrangian cobordisms.” In: *Journal of the European Mathematical Society (JEMS)* 18.11 (2016), pp. 2627–2689 (↑ 8).
- [EF98] Yakov Eliashberg and Maia Fraser. “Classification of topologically trivial Legendrian knots.” In: *Geometry, Topology, and Dynamics (Montreal, PQ, 1995)*. Vol. 15. CRM Proceedings and Lecture Notes. American Mathematical Society, Providence, RI, 1998, pp. 17–51 (↑ 8).
- [EM02] Yakov Eliashberg and Nikolai Mishachev. *Introduction to the h-principle*. Vol. 48. Graduate Studies in Mathematics. American Mathematical Society, Providence, RI, 2002, pp. xviii+206 (↑ 9).
- [Etn+23] John B. Etnyre, Hyunki Min, Lisa Piccirillo, and Agniva Roy. “Small symplectic caps and embeddings of homology balls in the complex projective plane.” In: *arXiv preprint arXiv:2305.16207* (2023) (↑ 5).
- [GK16] David Gay and Robion Kirby. “Trisecting 4-manifolds.” In: *Geometry & Topology* 20.6 (2016), pp. 3097–3132 (↑ 1).
- [GM22] David Gay and Jeffrey Meier. “Doubly pointed trisection diagrams and surgery on 2-knots.” In: *Mathematical Proceedings of the Cambridge Philosophical Society* 172.1 (2022), pp. 163–195 (↑ 2).
- [Giv86] Aleksandr Borisovich Givental. “Lagrangian imbeddings of surfaces and unfolded Whitney umbrella.” In: *Functional Analysis and Its Applications* 20.3 (1986), pp. 197–203 (↑ 20, 25).
- [GL24] Devashi Gulati and Peter Lambert-Cole. “Moduli Spaces of Lagrangian Surfaces in $\mathbb{C}\mathbb{P}^2$ obtained from Triple Grid Diagrams.” In: *arXiv preprint arXiv:2406.12767* (2024) (↑ 24).
- [HKM20] Mark C. Hughes, Seungwon Kim, and Maggie Miller. “Isotopies of surfaces in 4-manifolds via banded unlink diagrams.” In: *Geometry & Topology* 24.3 (2020), pp. 1519–1569 (↑ 2, 20).
- [Lam23] Peter Lambert-Cole. “Symplectic surfaces and bridge position.” In: *Geometriae Dedicata* 217.8 (2023) (↑ 2).
- [MZ17] Jeffrey Meier and Alexander Zupan. “Bridge trisections of knotted surfaces in S^4 .” In: *Transactions of the American Mathematical Society* 369.10 (2017), pp. 7343–7386 (↑ 2, 20).

- [MZ18] Jeffrey Meier and Alexander Zupan. “Bridge trisections of knotted surfaces in 4-manifolds.” In: *Proceedings of the National Academy of Sciences* 115.43 (2018), pp. 10880–10886 (↑ 2, 20).
- [Nem09] Stefan Yurievich Nemirovski. “Homology class of a Lagrangian Klein bottle.” In: *Izvestiya: Mathematics* 73.4 (2009), pp. 689–698 (↑ 20).
- [She09] Vsevolod V. Shevchishin. “Lagrangian embeddings of the Klein bottle and combinatorial properties of mapping class groups.” In: *Izvestiya: Mathematics* 73.4 (2009), pp. 797–859 (↑ 20).

DEPARTMENT OF MATHEMATICS, UNIVERSITY OF VIRGINIA, CHARLOTTESVILLE, VA 22904

Email address: blackwell@virginia.edu

URL: <https://seblackwell.com/>

DEPARTMENT OF MATHEMATICS, UNIVERSITY OF GEORGIA, ATHENS, GA 30602

Email address: dgay@uga.edu

DEPARTMENT OF MATHEMATICS, UNIVERSITY OF GEORGIA, ATHENS, GA 30602

Email address: plc@uga.edu